ACS OMEGA

http://pubs.acs.org/journal/acsodf

Article

Effects of Au States in Thiol-Organosilica Nanoparticles on Enzyme-like Activity for X-ray Sensitizer Application: Focus on Reactive Oxygen Species Generation in Radiotherapy

Chihiro Mochizuki, Junna Nakamura, and Michihiro Nakamura*

Cite This: *ACS Omega* 2023, 8, 9569–9582

Read Online

ACCESS | Metrics & More | Article Recommendations | Supporting Information

ABSTRACT: In radiotherapy, the use of Au nanoparticles (Au NPs) has been proposed to enhance cell damage by X-ray irradiation. Although the role of Au in radiotherapy is not fully understood, the catalytic activity of Au has been actively studied in the industrial field. Moreover, owing to their enzyme-like activity and high biocompatibility *in vitro* and *in vivo*, Au NPs present significant potential for biological applications. In this study, we incorporated different Au states both on the surface and embedded in thiol-organosilica (thiol-OS/Au series) to investigate the efficiency of anticancer cell activity of Au in radiotherapy. The thiol-OS/Au series comprised different Au(I)/Au(0) ratios and Au NPs, and different sizes of Au NPs were embedded in thiol-OS/Au. These thiol-OS/Au series samples were evaluated for enzyme-like activities in reactive oxygen species (ROS) generation by X-ray irradiation. Thiol-OS/Au embedded with small Au NPs (AC600/thiol-OS/Au) exhibited peroxidase (POD)-like activity under acidic conditions. This POD-like activity improved ROS generation and cytotoxicity under X-ray irradiation. Furthermore, AC600/thiol-OS/Au exhibited catalase (CAT)-like activity under basic conditions and showed no cytotoxicity toward nonirradiated cells. These results revealed the efficiency of functionalizing with small Au NPs that possess pH-controlled POD- and CAT-like activity as a radiosensitizer. We compared the suitability of using Au with different states to obtain the thiol-OS/Au series samples for application as radiosensitizers. The findings of this study will aid the design of efficacious strategies for the Au nanostructure-based radiotherapy of cancer cells.

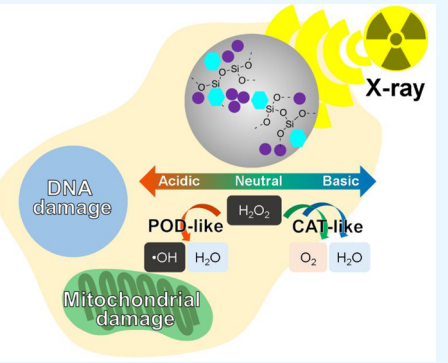

INTRODUCTION

Radiation therapy is an effective cancer treatment used for common tumors in combination with chemotherapy, surgery, and immunotherapy.[1] Radiation therapy uses ionizing radiation (IR), which consists of electromagnetic waves (X-rays and γ-rays) and particle rays (alpha, beta, and neutron rays). IR-induced cell death occurs via the interaction between IR and biomolecules, which leads to ionization and excitation, producing reactive oxygen species (ROS), such as hydroxyl radical (·OH) and superoxide anion radical ($O_2\cdot^-$).[2] ROS, such as $O_2\cdot^-$, H_2O_2, and ·OH, are continuously produced as byproducts of metabolic processes in living organisms. Typically, the produced excess ROS are also scavenged during metabolic processes.[3,4] However, excess IR-induced ROS can also react with cellular components, causing protein denaturation and deoxyribonucleic acid (DNA) damage.[5] Subsequently, the damaged cells are repaired in a series of cell processes; however, unsuccessful cell repair can cause cell death within several days. Although high-dose X-ray irradiation effectively kills cancer cells, the high radiation dosage causes concerning side effects, necessitating the improved efficacy of low-dose X-ray irradiation. In this regard, combining low-dose X-ray irradiation with radiosensitizers, which are drugs or chemical compounds that enhance the lethal effects of radiation, has been considered an effective treatment strategy for malignant cells using radiation therapy.

Thiol-organosilica (thiol-OS) NPs have been considered drug delivery system carriers because of their size controllability, biocompatibility, stability, and multifunctionality.[6] In our previous reports, size-controlled thiol-OS NPs have been successfully prepared from thiol-organosilicate using a one-pot synthesis.[7] Thiol-OS NPs were internally and surface-functionalized with various functional molecules, such as fluorescent dyes,[8] and applied for fluorescent imaging *in vivo*[9] and *in vitro*.[10] Also, we demonstrated the effect of Au nanoparticle (Au NP) surface functionalization of thiol-OS NPs in radiotherapy as the theranostics NPs.[11]

Au NPs have been applied for radiation therapy owing to their radiosensitization properties. Au NPs increase X-ray photoelectric absorption in cells, which is in accordance with the high-Z material theory.[12] However, the mechanism behind the IR

Received: January 6, 2023
Accepted: February 23, 2023
Published: March 3, 2023

https://doi.org/10.1021/acsomega.3c00096
ACS Omega 2023, 8, 9569–9582

effects of Au NPs remains unclear. Previous studies have demonstrated chemical enhancement under X-ray irradiation using Au NPs with small diameters as radiosensitizers.[13] This size effect of Au NPs differs from that of catalytic reactions of Au NPs, where the increase in the number of surface Au atoms improves the catalytic efficiency. Contrarily, several studies have demonstrated that the radiosensitization effect of Au NPs in radiation therapy is not only due to ROS production by X-ray irradiation but also because of the increased ROS level owing to the catalytic activity of Au NPs.[14] The increase in intracellular ROS levels causes oxidative stress, resulting in cellular damage and cell death.[15−17] Thus, ROS production is a vital mechanism for cytotoxicity by inorganic and metal NP-induced cell death.

Small Au NPs supported on reducible metal oxide for CO oxidation and cationic Au supported on carbon for acetylene hydrochlorination were independently demonstrated by Haruta[18] and Hutchings[19] in the 1980s. Following this, the catalytic activity of Au has been investigated by many researchers.[20] Thus far, a size range of 0.5 to 5 nm has been considered optimal for Au NPs to exhibit catalytic activity; this is attributed to the increase in the population of low-coordinated Au atoms at the perimeter interface. Furthermore, the size effect on catalytic activity has been extrapolated for sphere-shaped Au NPs.[20] In the case of nonspherical Au NPs, the shape of Au NPs has been shown to affect the catalytic properties.[21]

Furthermore, Au NPs possess several enzyme-like activities similar to those of oxidoreductases, such as superoxide dismutase (SOD), peroxidase (POD), and catalase (CAT), mimicking the biological enzymes for applications in biochemistry.[22−25] The morphology and surface chemistry of Au NPs and external parameters, such as pH, affect the enzyme-like activity of Au NPs, thereby affecting the catalytic properties.[26,27] The SOD-like activity of Au NPs has been demonstrated in the decomposition of $O_2\cdot^-$. Au NPs coated with tannic acid exhibited SOD-like activity compared to Au NPs coated with polyvinylpyrrolidone, suggesting that the SOD-like activity was due to the antioxidant activity of tannic acid.[28] The POD-like activity of NPs was first observed in Fe-based NPs.[29] The POD-like activity of the positively charged Au NPs has also been reported. The Au NPs can oxidize the peroxidase substrate 3,3,5,5-tetramethylbenzidine (TMB) in the presence of H_2O_2, and the oxidized TMB (ox-TMB) develops a blue color in an aqueous solution.[30,31] Previously, Biswas et al. reported that Au nanorods with an aspect ratio of 2.8 were more catalytically active in TMB oxidation than cysteamine-capped Au NPs possessing a diameter of 34 nm.[32] McVey et al. also reported that smaller Au NPs with a diameter of 14 nm possessed higher catalytic activity,[33] implying that Au NPs with higher surface-to-volume ratios are more favorable for the catalytic reaction; in particular, the reaction occurs on the surface of Au NPs. Several studies demonstrated that the catalytic activity of Au NPs changes with differences in pH conditions.[27,34] In our previous study, POD-like activity was promoted under acidic conditions, and ROS was generated with H_2O_2 in cells that had absorbed Au NPs. When the pH was increased to 7, CAT-like activity became predominant.[27]

The enzyme-like catalytic activity of Au NPs can provide a synergistic effect for its application in radiation therapy. Therefore, investigating the enzyme-like catalytic activity of Au NPs in ROS generation can provide an appropriate design strategy for using Au NPs with ROS-generating ability as radiosensitizers in radiation therapy. Therefore, in this study, we investigated the enzyme-like catalytic activity in relation to ROS generation by X-ray irradiation for different controlled Au states in thiol-OS NPs. By incorporating Au NPs with different states on the surface and within thiol-OS, using the same particle source and controlled air calcination (AC) treatment at different temperatures, the effects of Au on radiation therapy were revealed (Figure 1).

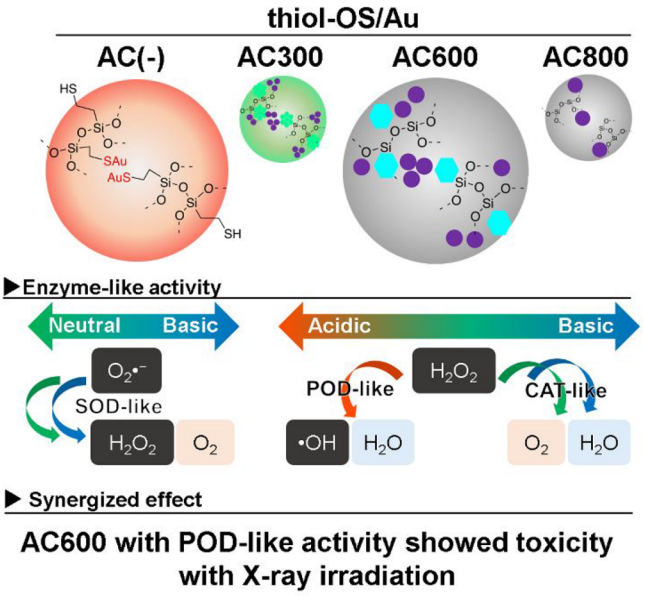

Figure 1. Schematic drawing of the thiol-OS/Au series for X-ray sensitizer for cancer cell therapy.

MATERIALS AND METHODS

Chemicals and Reagents. 3-Mercaptopropyltrimethoxysilane, bisbenzimide H 33342 trihydrochloride (Hoechst 33342), and branched polyethylenimine solution (MW = 2.0 k) were purchased from Sigma-Aldrich (St. Louis, MO, USA). 28% ammonium hydroxide (NH_4OH) and ethanol were purchased from Kishida Chemicals (Osaka, Japan). All reagents and solvents were of analytical grade.

Thiol-OS/Au series was characterized by transmission electron microscopy (TEM) and X-ray photoelectron spectroscopy (XPS). TEM images were recorded by a Tecnai G2 Spirit BioTWIN TEM instrument (FEI, Hillsboro, Oregon, USA) operated at 120 kV. XPS spectra were measured with a K-Alpha X-ray photoelectron spectrometer (Thermo Scientific, Waltham, Massachusetts, USA). The hydrodynamic sizes, polydispersities, and zeta potentials of thiol-OS/Au/polyethylenimine (PEI) series were measured using a DelsaMax PRO light scattering analyzer (Beckman Coulter Inc., Brea, California, USA) at 20 °C. The samples were dispersed in distilled water (DW) at a concentration of 0.1 mg/mL. The Au content in thiol-OS/Au was determined by inductively coupled plasma optical emission spectroscopy (ICP-OES) using Agilent 5100 (Agilent, California, USA). The samples were washed thrice times with DW. The sample was precipitated by centrifugation at 20,000*g* for 30 min, dried overnight at 100 °C, and solubilized in aqua regia (HCl/HNO_3) to measure the amount of Au in the samples.

Synthesis of Thiol-OS/Au Series. Thiol-OS/Au [AC (−)/thiol-OS/Au] was synthesized by a one-pot process as described previously.[35] The precipitate of thiol-OS/Au was dried under vacuum at 25 °C and calcined in air at 300, 600, or

https://doi.org/10.1021/acsomega.3c00096
ACS Omega 2023, 8, 9569−9582

800 °C for 2 h. The resulting products were named AC300/thiol-OS/Au, AC600/thiol-OS/Au, and AC800/thiol-OS/Au, respectively.

Surface Functionalization of Thiol-OS/Au Series with Polyethylenimine. Thiol-OS/Au (1 mg/mL) was mixed with 10% PEI in DW. The reaction solution was mixed for 24 h at 37 °C. After 24 h of mixing, the reaction solution was centrifuged at 20,000*g* for 20 min at 4 °C to remove the excess amounts of PEI; the pellet was washed three times with DW.

Electron Microscopic Observation. Thiol-OS/Au was dried over a 400-mesh copper grid (Nisshin EM Co., Tokyo, Japan) coated with poly(vinyl alcohol). TEM images of the NPs were recorded by a Tecnai G2 Spirit BioTWIN TEM (FEI, Hillsboro, Oregon, USA).

Enzyme-like Activity. *SOD-like Activity.* SOD-like activity was determined by an $O_2{\cdot}^-$/nitro blue tetrazolium (NBT) absorbance inhibition assay.[36] NBT was used as a probe for the quantification of $O_2{\cdot}^-$ concentration, by virtue of NBT reduction into a purple-colored formazan with an absorption peak at 560 nm. The reaction condition was as follows: acetate buffer, phosphate buffer, and borate buffer of pH 5.0, 7.4, and 9.0, respectively. The final concentration was fixed at 200 μM PMS reduced nicotinamide adenine dinucleotide (NADH), 3 μM phenazine methosulfate (PMS), and 50 μM NBT in 25 mM buffer solution. NPs were added to the appropriate amounts of thiol-OS/Au series. The reaction was conducted at 37 °C for 10 min, and the absorbance of the mixtures was recorded at 560 nm against a blank using a FlexStation 3 (Molecular Devices, USA) reader.

POD-like Activity. POD-like activity was evaluated by the oxidation of TMB.[30,37] TMB was used as the substrate for the oxidation, yielding oxidized TMB, a blue-colored solution with an absorption peak at 652 nm. The reaction condition was as follows: acetate buffer, phosphate buffer, and borate buffer of pH 5.0, 7.4, and 9.0, respectively. The final concentration was fixed at 800 μM TMB and 50 mM H_2O_2 in 10 mM buffer solution. NPs were added to the appropriate amounts of thiol-OS/Au series. After incubation at 37 °C for 15 min in the dark, the mixtures were immediately centrifuged at 30,000*g* for 5 min. The absorbance of the supernatants was measured at 652 nm using a FlexStation 3 reader (Molecular Devices, USA).

CAT-like Activity. The generation of O_2 was detected by a hypoxic fluorescent probe $[Ru(dpp)_3]Cl_2$.[38] The reaction condition was as follows: acetate buffer, phosphate buffer, and borate buffer of pH 5.0, 7.4, and 9.0, respectively. The final concentration was fixed at 10 μM $[Ru(dpp)_3]Cl_2$ and 50 mM H_2O_2 in 10 mM buffer solution. NPs were added in the appropriate amounts to thiol-OS/Au series. The reaction was conducted at 37 °C for 10 min. The fluorescence intensity (F.I.) changes of $[Ru(dpp)_3]Cl_2$ excited at 455 nm and detected at 613 nm using a FlexStation 3 reader (Molecular Devices, USA).

X-ray Irradiation. X-ray irradiation was conducted using an X-ray generator ([filter: 0.1 mm Cu and 0.5 mm Al] MBR-1520R-4, Hitachi, Japan).

Measurement of ROS Generation by X-ray Irradiation. The detection of hydroxyl radical (·OH) and superoxide anion radical ($O_2{\cdot}^-$) is based on the reaction between aminophenyl fluorescein (APF) and ·OH and dihydroethidium (DHE) and $O_2{\cdot}^-$, respectively. The ROS generation assays were measured in black microplates by a microplate reader (FlexStation 3, Molecular Devices, UK). The thiol-OS/Au series in DW were added to 5 or 50 μM APF or DHE. The mixed solutions were excited at 480 or 485 nm, and fluorescence was detected at 520 or 610 nm, respectively. The increase in the F.I. by X-ray irradiation was calculated by subtracting the F.I. from that blank (before X-ray irradiation).

Dynamic Light Scattering. Dynamic light scattering (DLS) was conducted to determine the size distribution and zeta potential of the thiol-OS/Au series by a DelsaMax PRO light scattering analyzer (Beckman Coulter, Brea, CA, USA) at 20 °C. The thiol-OS/Au series were prepared by dispersing them in DW (0.1 mg/mL).

Quantification of Cellular Uptake of Thiol-OS/Au Series by ICP-OES. The methods of quantification of cellular uptake of NPs by ICP-OES were described in our previous report.[11] Briefly, a total of 0.5×10^6 4T1 cells were seeded on 10 cm dishes and cultured at 37 °C for 24 h. The cells were incubated with 10 mL of thiol-OA/Au series containing medium (final concentration: 10 μg/mL) for 24 h. After 24 h of incubation, the cells were carefully washed three times with phosphate buffered saline [PBS (−)] and dispersed in 2 mL of PBS (−). The concentration of cells (cells/mL) was counted before the cell lysates. The cell samples were collected by centrifugation, lysed with 1 mL of aqua regia, and filled up to 2 mL by DW. The samples were measured by ICP-OES (5100 ICP-OES, Agilent Technologies, Mulgrave, Australia) to determine the number of NPs in the cell lysates. The several NPs in the cell lysate solution (2.0×10^6 cells/mL) were used as calibration curves.

Cell Viability Assay (WST-1 Assay). The evaluation methods of the cell viability assay (WST-1) were described previously.[11] 4T1 cells were seeded into 96-well plates at a density of 1000 cells per well under 100% humidity and cultured at 37 °C with 5% CO_2 for 24 h. Various concentrations of thiol-OS/Au series were added to the wells. After 24 h of NP treatment, the 4T1 cells took up the NPs and were irradiated with 8 Gy of X-ray; then, the 4T1 cells were incubated for 4 days with or without X-ray irradiation. The cell viability was analyzed by the WST-1 (2-(2-methoxy-4-nitrophenyl)-3-(4-nitrophenyl)-5-(2,4-disulfophenyl)-2*H*-tetrazolium) cell proliferation assay reagent (Dojin Chemical Co., Kumamoto, Japan). The WST-1 reagent was added to the wells 4 days after 8 Gy of X-ray irradiation.

Evaluation of Cell Count and Cell Viability. The evaluation methods of cell count and cell viability were described previously.[11] Briefly, a total of 0.4×10^5 4T1 cells were seeded into 35 mm dishes and cultured at 37 °C for 24 h. The 4T1 cells were incubated with thiol-OS/Au series (final concentration: 30 μg/mL) containing medium for 24 h. After 24 h of incubation, 4T1 cells were irradiated with 8 Gy of X-ray and incubated at 37 °C. After incubation, the cells were collected at the desired time (DAY 1 and DAY 4 after X-ray irradiation) and counted by a Vi-CELL (Beckman, Fullerton, CA, USA) with trypan blue.

DNA Double-Strand Breaks Imaging Assay. The evaluation of DNA double-strand breaks by fluorescence microscopy (FM) imaging was described previously.[11] Briefly, the 4T1 cells were seeded into a 96-well plate and incubated at 37 °C for 24 h. Subsequently, the NPs of the thiol-OA/Au series were added to the 96-well plate at a concentration of 30 μg/mL. After 24 h of incubation, the 4T1 cells were exposed 8 Gy of X-ray irradiation. The DNA double-strand breaks (DSBs) were evaluated by γ-H2AX immunofluorescence staining using a DNA damage detection kit (Dojin Chemical Co., Kumamoto, Japan) after 15 min of X-ray irradiation. 4′,6-Diamidino-2-phenylindole (DAPI) was used to stain the cell nuclei. The FM

https://doi.org/10.1021/acsomega.3c00096
ACS Omega 2023, 8, 9569−9582

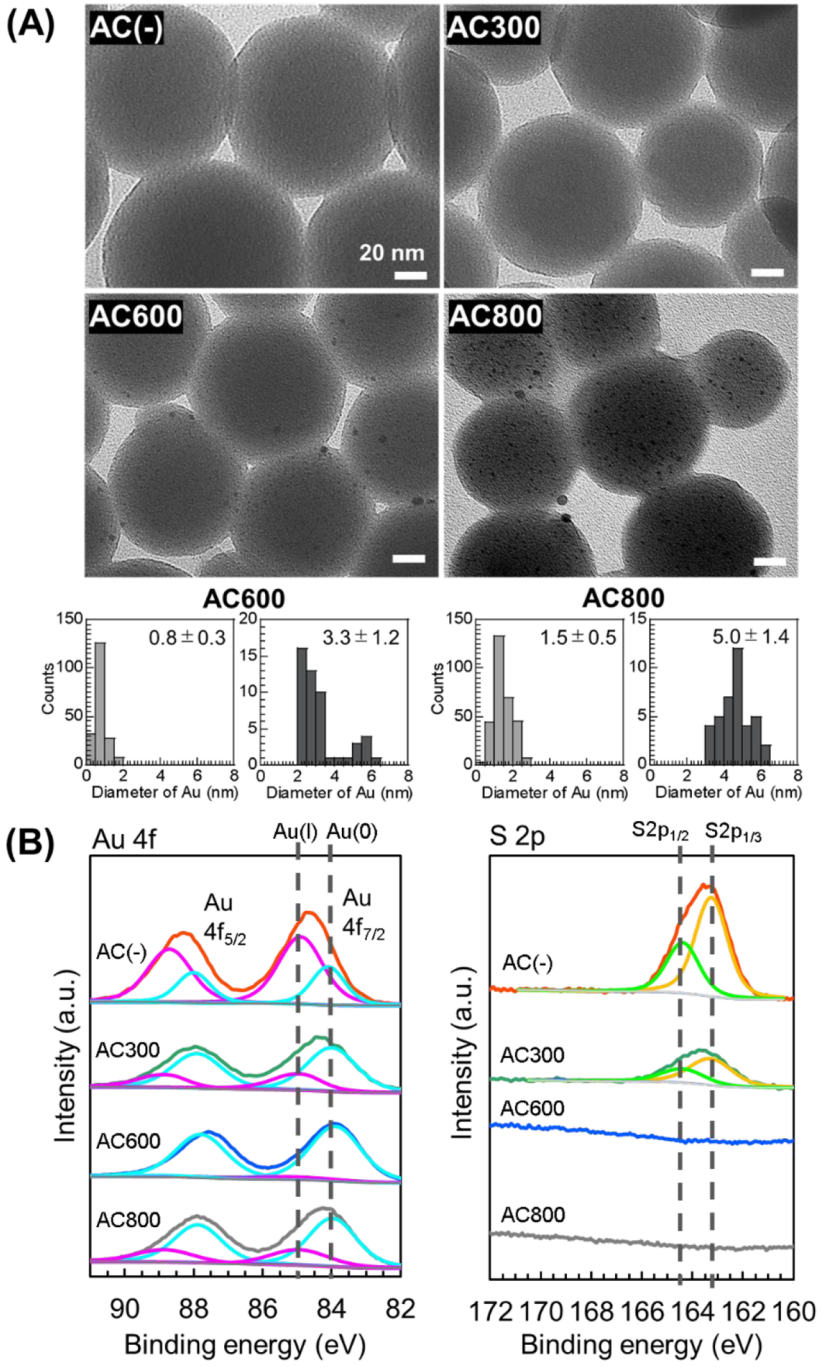

Figure 2. (A) TEM images of the thiol-OS/Au series. Scale bar = 20 nm. Size distribution of Au NPs in AC600/thiol-OS/Au and AC800/thiol-OS/Au. Particle size distribution for smaller and larger Au NPs was estimated using 200 and 50 particles, respectively. (B) XPS spectra of thiol-OS/Au series.

images were recorded using a BZ-X800 (Keyence, Osaka, Japan), and the γ-H2AX expression of cells per all cells was analyzed by Hybrid Cell Count BZ analyzer software (Keyence, Osaka, Japan).

Evaluation of Mitochondrial Activity. The evaluation of mitochondrial activity by FCM was described previously.[11] Briefly, cell culture and X-ray irradiation were conducted in a similar manner to the cell counts and viability evaluation. All cells were collected after the incubation. The cells in the supernatant were carefully separated by trypsin, collected by centrifugation at 1,000*g* for 10 min at 25 °C, redispersed, stained with tetramethylrhodamine ethyl ester perchlorate (TMRE, Invitrogen, Eugene, OR, USA), and subjected to flow cytometry (FCM) analysis. The FCM was conducted by a FACSCalibur flow cytometer with Cell Quest (Becton Dickinson, San Jose, CA, USA) and 488 nm excitation lasers [5,000 cells, FL2 channel (542−627 nm)].

Statistical Analysis. All data, which are herein presented as the mean ± standard deviation (SD) from three replicates, were analyzed by one-way analysis of variance followed by the Tukey−Kramer test in Microsoft Excel; statistical significance was set at $^{*}P < 0.05$ and $^{**}P < 0.01$.

https://doi.org/10.1021/acsomega.3c00096
ACS Omega 2023, 8, 9569−9582

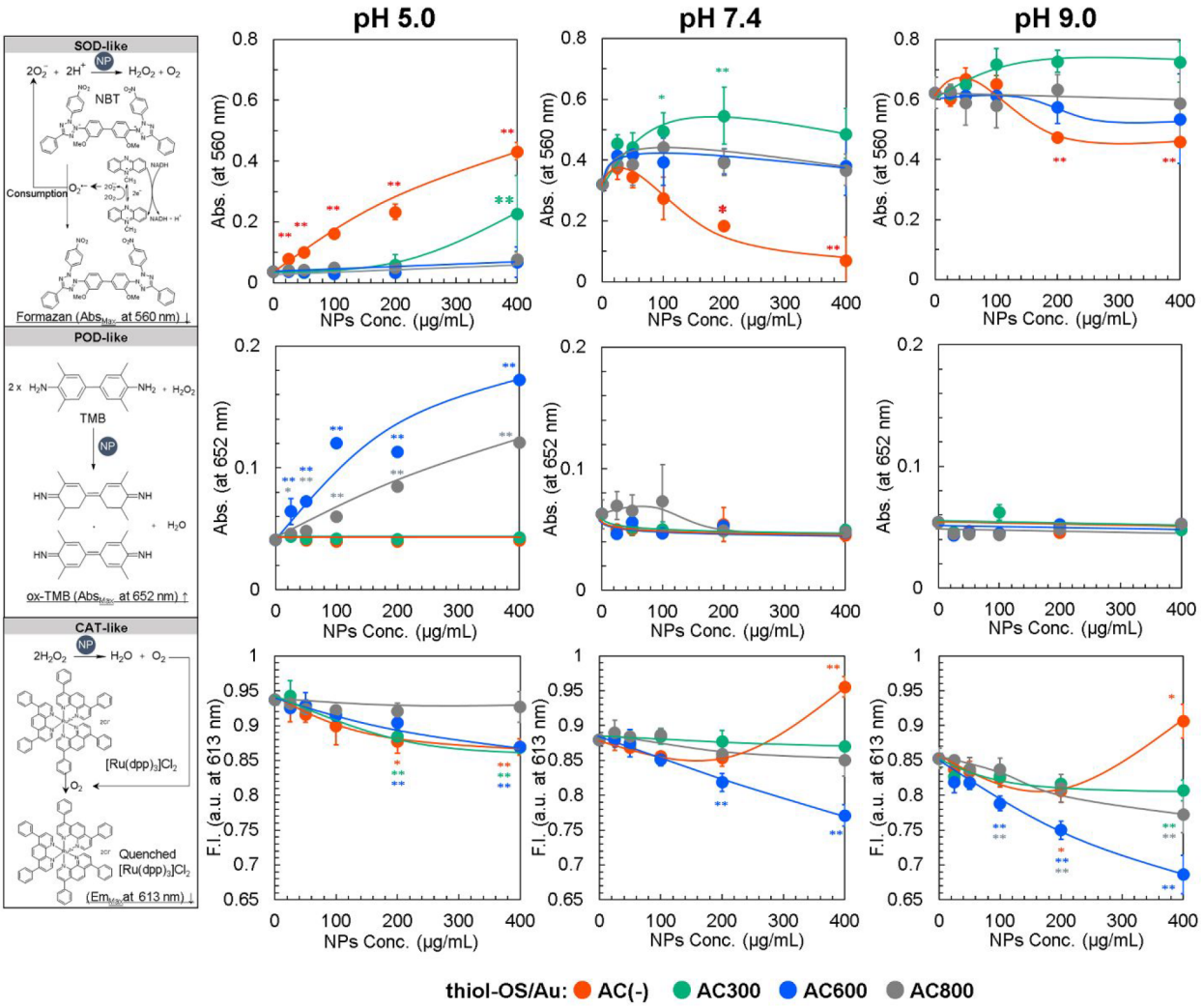

Figure 3. Enzyme-like activity of the thiol-OS/Au series at different pH values. The concentrations of NPs represent those before the AC treatment of thiol-OS/Au [AC (−)/thiol-OS/Au]; the concentration of Au was fixed in the thiol-OS/Au series. Each value represents mean ± SD, where $n = 3$. *: Significantly different from the F.I. with 0 μg/mL of NPs.

RESULTS AND DISCUSSION

Synthesis and Characterization of Au Valence States of the Thiol-OS/Au Series. A thiol-OS/Au series, comprising samples with different Au states embedded in thiol-OS NPs, was synthesized as described in a previous study.[35] Thiol-OS NPs have been applied for biological and medical applications, such as multimodal imaging and targeting, via the multifunctionalization of NPs.[6,39] Figure 2A shows TEM images of the thiol-OS/Au series. TEM images reveal that the thiol-OS/Au samples retain a uniform contrast, and no distinct structures are observed in thiol-OS/Au and AC300/thiol-OS/Au. In our previous study, AC300/thiol-OS/Au contained oligomeric Au(I)−thiolate complex states of Au.[35] AC600/thiol-OS/Au and AC800/thiol-OS/Au clearly show particulate structures, indicated by the dark contrast images. These TEM images suggest the formation of Au NPs owing to the increased AC treatment temperature. Two types of Au NP size distribution are observed for AC600/thiol-OS/Au and AC800/thiol-OS/Au, which indicates that the surface of Au aggregates easily compared to the interior of Au. The average diameters of the Au NPs in AC600/thiol-OS/Au and AC800/thiol-OS/Au estimated using TEM are 0.8 ± 0.3 nm/3.3 ± 1.2 nm and 1.5 ± 0.5 nm/5.0 ± 1.5 nm, respectively (in Figure 2A), suggesting that an increase in the AC treatment temperature causes the aggregation of Au NPs.

The oxidation state of Au in the thiol-OS/Au series was measured by XPS (Figure 2B).[35] The XPS spectrum of Au 4f is deconvoluted into two components centered at the binding energies of 84.0 and 85.0 eV, which are assigned to Au(0) and Au(I), respectively.[40] The thiol-OS/Au, AC300/thiol-OS/Au, AC600/thiol-OS/Au, and AC800/thiol-OS/Au contained 67.1%, 27.5%, 7.4%, and 29.1% of Au(I), respectively. The XPS spectrum of S 2p is deconvoluted into two components at binding energies of 164 and 168 eV, which are attributed to −SH or −SS− and oxidized sulfur ($-SO_x$), respectively. The XPS spectrum of thiol-OS/Au exhibits a peak at approximately 164 eV, which is assigned to reduced sulfur species.[41] The spectrum of AC300/thiol-OS/Au indicates the presence of reduced sulfur species, whereas no oxidized sulfur species are observed, and AC600/thiol-OS/Au and AC800/thiol-OS/Au do not show the presence of sulfur species. Furthermore, AC (−)/thiol-OS/Au contained 14.7% (w/w) of Au, as determined via ICP-OES measurements. To evaluate the effects of Au on X-ray-sensitizing abilities, the samples were fixed at the amounts of Au content for subsequent experiments.

https://doi.org/10.1021/acsomega.3c00096
ACS Omega 2023, 8, 9569−9582

Enzyme-like Activity of the Thiol-OS/Au Series. ROS, such as $O_2{\cdot}^-$, H_2O_2, and ·OH, are generated as byproducts of cellular metabolic processes. Among them, the free radicals with unpaired electrons, such as $O_2{\cdot}^-$ and ·OH, have short lifetimes and high reactivity and disrupt the structure and function of proteins, nucleic acids, carbohydrates, and other substances.[34] The enzyme-like activity of Au NPs has been confirmed, and the catalytic activities depend on the morphology of Au NPs. Similar to biological enzymes, reactions catalyzed by Au nanozymes require favorable pH and temperature control. Therefore, several NP parameters (i.e., Au state, size, and morphology) and environmental factors, such as pH, can strongly affect the catalytic properties. Therefore, we investigated the effects of Au states and NP size on the efficiency of the enzyme-like activity of Au under different pH conditions.

SOD catalyzes the dismutation of $O_2{\cdot}^-$ into O_2 and H_2O_2 as an antioxidant against oxidative stress in the living systems. A previous study showed that Au NPs efficiently catalyzed the decomposition of $O_2{\cdot}^-$, indicating that Au NPs can act as SOD mimetics. SOD-enzyme-like activities were determined using the classic method of the $O_2{\cdot}^-$/ NBT absorbance inhibition assay.[36] As shown in Figure 3, AC (−)/thiol-OS/Au exhibits NP concentration-dependent SOD-like activities at pH 7.4. Approximately 45% and 79% of the total $O_2{\cdot}^-$ content was inhibited by 200 and 400 μg/mL of AC (−)/thiol-OS/Au, respectively; the calculated absorbance (Abs.) at 560 nm decreased from 0.33 to 0.18 and 0.07, respectively. The SOD-like activity was tested for thiol-OS NPs (without Au) at pH 7.4 to further confirm the effects of Au in thiol-OS NPs on enzyme-like activity (Figure S1). This result suggests that thiol-OS NPs did not show SOD-like activity but instead generated $O_2{\cdot}^-$. Hence, the SOD-enzyme-like activity is caused by the presence of Au NPs. Additionally, studies on enzyme-like activities of thiol-OS NPs are ongoing. AC300/thiol-OS/Au did not exhibit SOD-like activities, and the generation of $O_2{\cdot}^-$ was observed at pH 7.4. This tendency is also observed for thiol-OS NPs without Au (Figure S2). A control experiment was conducted for the thiol-OS/Au series under only-NBT conditions to confirm the interaction between NBT and NPs (Figure S2), showing that the thiol-OS/Au series did not interact with NBT. In the $O_2{\cdot}^-$/ NBT absorbance inhibition assay, $O_2{\cdot}^-$ was chemically generated by the PMS and reduced NADH system. The increase in the generation of $O_2{\cdot}^-$ by AC300/thiol-OS/Au and thiol-OS NPs could be further promoted by reducing NAD to NADH in the presence of NPs. In the case of AC600/thiol-OS/Au and AC800/thiol-OS/Au, the SOD-like activities were not observed at pH 7.4. The increase in the generation of $O_2{\cdot}^-$ at pH 9.0 compared to that at pH 7.4 in the absence of NPs was confirmed, suggesting that the generation of $O_2{\cdot}^-$ by the PMS and NADH system was promoted under the basic reaction condition. At pH 5.0, $O_2{\cdot}^-$ generation by PMS and the NADH system was not observed. These results suggest that the SOD-like activity of thiol-OS/Au series could not be evaluated at pH 5.0. On the other hand, thiol-OS/Au and AC300/thiol-OS/Au generated $O_2{\cdot}^-$ at pH 5.0 because the increase of Abs. at 560 nm was observed.

PODs, comprising ferric heme proteins, catalyze substrate oxidation by consuming H_2O_2. Many Fe-based nanomaterials have been observed to possess POD-like activity. The POD-like activity was evaluated by the oxidation of the POD substrate TMB with H_2O_2. The ox-TMB developed a blue color in an aqueous solution. As shown in Figure 3, AC600/thiol-OS/Au and AC800/thiol-OS/Au exhibited NP concentration-dependent POD enzyme-like activity. However, the POD enzyme-like activity of AC600/thiol-OS/Au is higher than that of AC800/thiol-OS/Au at pH 5.0. AC600/thiol-OS/Au shows a substantial increase in Abs. from 0.04 to 0.06 at 652 nm, even at an NP concentration of 25 μg/mL. AC800/thiol-OS/Au also shows a considerable increase in Abs. at 652 nm for an NP concentration of 100 μg/mL. However, AC (−)/thiol-OS/Au and AC300/thiol-OS/Au do not exhibit POD enzyme-like activity at pH 5.0. From the point of Au valency, AC300/thiol-OS/Au and AC800/thiol-OS/Au possess similar values but the POD-like activity was different, suggesting the nanoparticle state of Au would be more favorable for the POD-like activity. At pH 7.4 and 9.0, the POD-enzyme-like activity is not observed for all the thiol-OS/Au series. Considering POD-like activity, AC600/thiol-OS/Au shows higher activity than AC800/thiol-OS/Au because AC600/thiol-OS/Au possesses Au NPs smaller than those of AC800/thiol-OS/Au, indicating the size effects of Au on catalytic activity.[20]

CAT decomposes H_2O_2, which is formed from $O_2{\cdot}^-$ by the SOD in the cells, into O_2 and H_2O. The CAT-like activity was evaluated using tris(4,7-diphenyl-1,10-phenanthroline) ruthenium(II) dichloride ($[Ru(dpp)_3]Cl_2$), which is an O_2-quenching fluorescent probe.[38] As shown in Figure 3, AC600/thiol-OS/Au exhibits significant activity, whereas AC800/thiol-OS/Au exhibits a slight activity at pH 9.0 in a NP concentration-dependent manner. The activity for AC600/thiol-OS/Au is higher than that of AC800/thiol-OS/Au at pH 9.0. AC600/thiol-OS/Au also exhibits CAT-like activity at pH 7.4. However, except AC800/thiol-OS/Au, all other samples exhibit slight CAT-like activity at pH 5.0. Li et al. reported the pH-switchable POD- and CAT-like activities of Au NPs.[27] The POD-like activity was promoted under acidic conditions with H_2O_2 in Au NPs. When pH increased to neutral pH values, the CAT-like activity became predominant.[42] Our results also showed the pH-switchable POD- and CAT-like activities. However, at pH 9.0 and 7.4, thiol-OS/Au shows an increase in the F.I., suggesting that the quenched $[Ru(dpp)_3]Cl_2$ is recovered in the presence of thiol-OS/Au.

From the perspective of a ROS scavenger, SOD- and CAT-like activities are antioxidant defenses in cells exposed to $O_2{\cdot}^-$ and H_2O_2, respectively. In a previous study, Au NPs assembled on nano-CeO_2 have shown SOD- and CAT-like activities.[43] These enzymes possess complementary functions, whereby the toxic intermediates (H_2O_2) generated by SOD can be promptly eliminated by CAT in the cell. Consequently, the combined action of SOD and CAT has been shown to scavenge ROS effectively. Thiol-OS/Au showed SOD-like activity at pH 7.4, revealing antioxidant ability. However, AC600/thiol-OS/Au showed POD-like activity by generating ·OH in acidic environments in the presence of H_2O_2, which may facilitate the oxidation of intracellular components in the cell.[23] From these enzyme-like catalytic activities, AC600/thiol-OS/Au is absorbed in the cells via endocytosis; the system acquires an acidic pH because the absorbed NPs move from endosomes to lysosomes. Therefore, ·OH can be generated in cells with acidic pH through the catalytic activity of AC600/thiol-OS/Au. Additionally, solid tumors are dependent on acidic pH owing to the Warburg effect, which is known for the highly enhanced glycolysis of tumor cells.[44] Therefore, AC600/thiol-OS/Au can be expected to be more favorable to generate ·OH in a cancer cell environment.

ROS Generation of Thiol-OS/Au Series by X-ray Irradiation. The IR of water and oxygen generates ROS (i.e.,

https://doi.org/10.1021/acsomega.3c00096
ACS Omega 2023, 8, 9569−9582

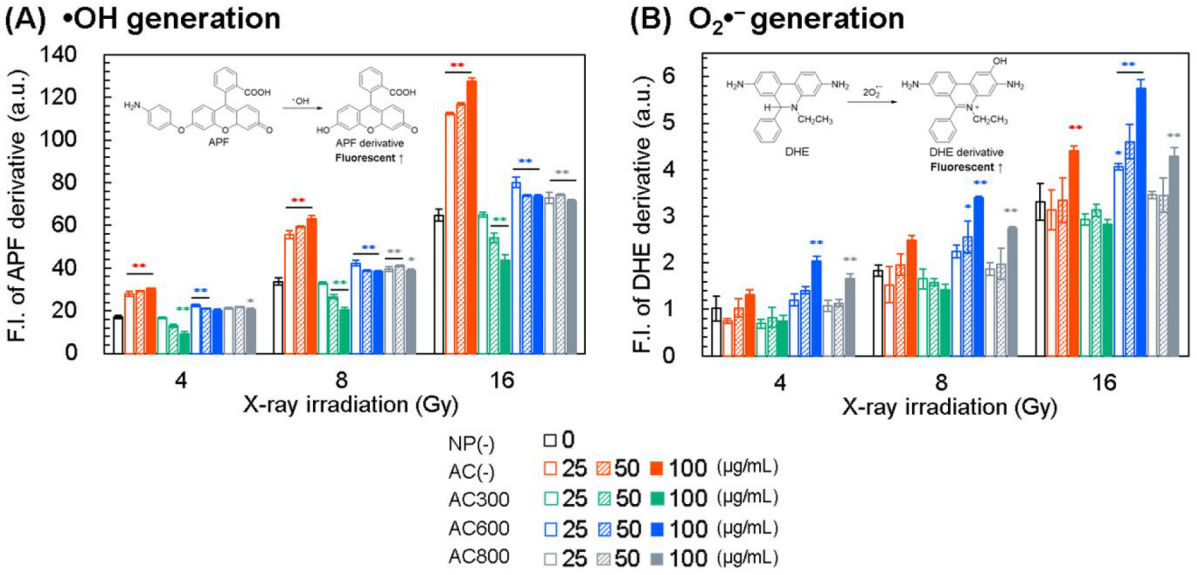

Figure 4. ROS generation for (A) ·OH and (B) O_2·⁻ of thiol-OS/Au under different X-ray irradiation conditions. The concentration of NPs represents AC (−)/thiol-OS/Au; the concentration of Au was fixed in the thiol-OS/Au series. Each value represents mean ± SD, where n = 3. *: Significantly different from the F.I. with 0 μg/mL of NPs.

·OH and O_2·⁻). A previous study showed that the presence of Au NPs in water increases the production of ·OH and O_2·⁻ by 1.46- and 7.68-fold, respectively, by X-ray irradiation, suggesting that the surface area of Au NPs enhanced ROS generation.[45] Our previous study also showed the increase in ·OH generation owing to the Au NP functionalization of thiol-OS.[11] In this study, we investigated the X-ray-sensitizing ability of the thiol-OS/Au series by measuring the ·OH and O_2·⁻ generation (Figure 4). The generation of ·OH and O_2·⁻ was measured using the F.I. of APF and DHE derivatives, which interact with ·OH and O_2·⁻, respectively.

In the case of ·OH generation, the F.I. of the APF derivative increased in an X-ray dose-dependent manner without NPs (NP (−)). First, we evaluated the concentration effect of NPs on the X-ray-sensitizing ability for the thiol-OS/Au series at 4, 8, and 16 Gy irradiation. The F.I. of the APF derivative for AC (−)/thiol-OS/Au substantially increased in an NP concentration-dependent manner at 4, 8, and 16 Gy X-ray irradiation. Compared to NP (−), the F.I. increased from 64 to 112, 117, and 128 when the NP concentration was increased to 25, 50, and 100 μg/mL, respectively, at 16 Gy irradiation. Next, the F.I. of the APF derivative for AC300/thiol-OS/Au decreased at high concentrations of NPs compared to that of NP (−) at 4, 8, and 16 Gy X-ray irradiation. Furthermore, the F.I. of the APF derivative for AC600/thiol-OS/Au and AC800/thiol-OS/Au showed a slight increase but did not show the NP concentration-dependent trend at 4, 8, and 16 Gy X-ray irradiation. These results show that the F.I. of the APF derivative increases in AC (−)/thiol-OS/Au, suggesting that the Au(I) state or highly dispersed Au state is more favorable for the generation of ·OH than the nanoparticulate Au state.

Considering O_2·⁻ generation, the F.I. of the DHE derivative increased in an X-ray dose-dependent manner without NPs (NP (−)). The effect of the NP concentration on the generation of O_2·⁻ at 4, 8, and 16 Gy irradiation was evaluated for the thiol-OS/Au series. First, the F.I. of the DHE derivative for AC600/thiol-OS/Au considerably increased in an NP concentration-dependent manner at 4, 8, and 16 Gy X-ray irradiation. Compared to NP (−), the F.I. increased from 3.31 to 4.06, 4.60, and 5.76 when the NP concentration was increased to 25, 50, and 100 μg/mL, respectively, at 16 Gy of X-ray irradiation. The F.I. of the DHE derivative for AC (−)/thiol-OS/Au and AC800/thiol-OS/Au also increased at a high NP concentration. However, the F.I. of the DHE derivative for AC300/thiol-OS/Au did not show any significant increase upon X-ray irradiation. These results indicate that the F.I. of the DHE derivative increases in the thiol-OS/Au series, except for AC300/thiol-OS/Au, under the NP (−) condition. The X-ray-sensitizing ability for AC600/thiol-OS/Au was higher than that of AC (−)/thiol-OS/Au and AC800/thiol-OS/Au.

The main ROS product formed upon X-ray irradiation is ·OH, which causes water radiolysis in a water solution system. Therefore, thiol-OS/Au produces ROS effectively upon X-ray irradiation.

Cellular Uptake of Thiol-OS/Au/Polyethylenimine (PEI) Series. In our previous study, the PEI modification of NPs remarkably enhanced the uptake of NPs for 4T1 cells.[11] 4T1 cells are known as a triple-negative mouse breast cancer cell line and have been used to evaluate the effect of NPs.[46,47] In addition, radiotherapy is important for managing metastatic triple-negative breast cancer. The mean diameters, hydrodynamic sizes, and zeta potentials of the thiol-OS/Au/PEI series are shown in Table 1. The hydrodynamic diameter is 181−189 nm, showing only a slight difference in the thiol-OS/Au series. The zeta potential of the thiol-OS/Au series is negative and shifts from −33 ± 2 [AC (−)/thiol-OS/Au] to −17 ± 1 (AC800/thiol-OS/Au), as listed in Table S1, which is attributed to the lower number of thiol groups on the surface of NPs owing to oxidative decomposition.[35] To accelerate cellar uptake for 4T1 cells, we functionalized the thiol-OS/Au series with PEI. The PEI-functionalized thiol-OS/Au series showed a positive zeta potential owing to the PEI functionalization with the amino group moiety. The zeta potentials of AC (−)/thiol-OS/Au/PEI and AC300/thiol-OS/Au/PEI are 37 ± 0 and 39 ± 1 mV, respectively, indicating no considerable difference. The zeta potentials of AC600/thiol-OS/Au/PEI and AC800/thiol-OS/Au/PEI are 24 ± 1 and 18 ± 1 mV, respectively. These results suggest that the extent of PEI functionalization is more in thiol-

https://doi.org/10.1021/acsomega.3c00096
ACS Omega 2023, 8, 9569−9582

Table 1. Hydrodynamic Diameters and Zeta Potentials of the Thiol-OS/Au/PEI Series via DLS Measurements and the Quantification of the Au Cellular Uptake for the Thiol-OS/Au/PEI Series Determined Using ICP-OES Measurements

	DLS		ICP-OES
	hydrodynamic diameter[a] ± polydispersity (nm)	zeta potential[b] (mV)	Au (pg/cell)
AC (−)/thiol-OS/Au/PEI	187 ± 60	37 ± 1	0.45 ± 0.14
AC300/thiol-OS/Au/PEI	182 ± 71	39 ± 1	0.47 ± 0.05
AC600/thiol-OS/Au/PEI	181 ± 51	24 ± 1	0.26 ± 0.04
AC800/thiol-OS/Au/PEI	189 ± 63	18 ± 1	0.23 ± 0.07

[a]Hydrodynamic diameter and polydispersity are estimated via DLS measurements. [b]Values represent the average of three DLS measurements.

OS/Au/PEI and AC300/thiol-OS/Au/PEI than that in AC600/thiol-OS/Au/PEI and AC800/thiol-OS/Au/PEI, which are affected by the negatively charged zeta potentials of the bare thiol-OS/Au series because of the interaction between NPs and PEI caused by electrostatic attraction.

The Au concentration originated from NPs in 4T1 cells is shown in Table 1, as quantified using ICP-OES measurements. The quantity of absorbed Au (pg/cell), based on all the cells that absorbed the NPs, was calculated from the results of ICP-OES; the number of cells was counted before cell lysis. The Au concentration uptake per 4T1 cells for AC (−)/thiol-OS/Au/PEI, AC300/thiol-OS/Au/PEI, AC600/thiol-OS/Au/PEI, and AC800/thiol-OS/Au/PEI was 0.45, 0.47, 0.26, and 0.23 pg/cell, respectively. These results indicate that more positively charged PEI-functionalized NPs accelerate the cellular uptake of 4T1 cells.

DNA Damage by the Thiol-OS/Au Series upon X-ray Irradiation. IR can induce direct and indirect DNA damage, which includes the generation of ·OH and $O_2^{\cdot -}$ clusters by radiolysis. DNA DSBs are a fatal type of DNA damage. During the early stages of cellular DSBs, the histone H2A variant H2AX is phosphorylated at the sites of DNA damage, resulting in γ-H2AX (phosphorylated H2AX) at the sites of the DNA damage. Therefore, we assessed DNA damage via the γ-H2AX immunofluorescence staining.

Figure 5A shows the FM images of 4T1 cells after 15 min of X-ray irradiation. The cell nuclei and γ-H2AX were stained blue with DAPI and magenta with Cy5 for fluorescence, respectively. For untreated NP (NP (−)) cells (treated with 0 Gy as the double negative control), a negligible γ-H2AX concentration was observed in the cell nuclei. Additionally, the γ-H2AX signals of the thiol-OS/Au series-treated 4T1 cells with 0 Gy are also not observed, suggesting that all the thiol-OS/Au samples do not damage the cell nuclei without X-ray. However, with 8 Gy irradiation, the fluorescence signal of γ-H2AX is clearly detected in the nucleus in NP (−) and all thiol-OS/Au samples. The number of damaged cells and F.I. of stained γ-H2AX per DAPI area are determined as shown in Figure 5B. In the case of 0 Gy irradiation, the percentage of damaged cells and F.I. of γ-H2AX

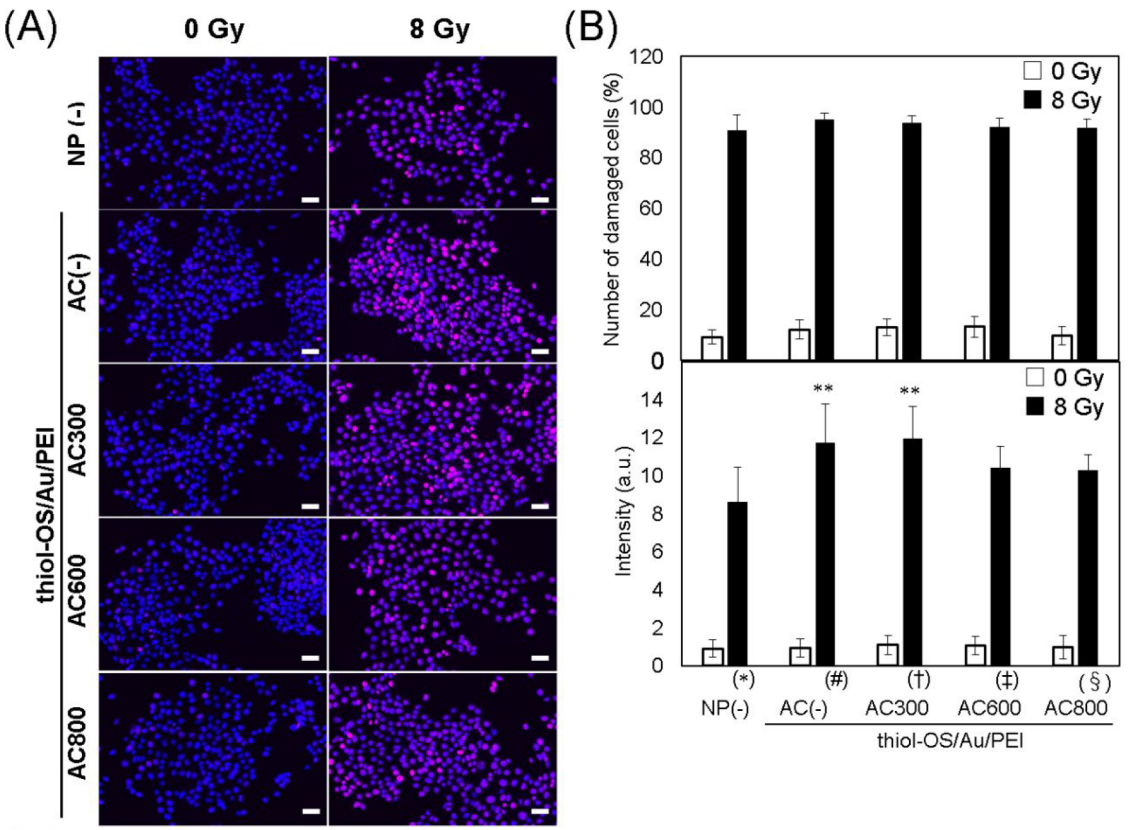

Figure 5. FM images (scale bar = 50 μm) (A) and γ-H2AX expression (B) of 4T1 cells before and after treatment with 30 μg mL^{-1} of the thiol-OS/Au/PEI series upon 0 and 8 Gy X-ray irradiation after 15 min. Concentration of NPs represents AC (−)/thiol-OS/Au, implying that the concentration of Au is fixed in the thiol-OS/Au/PEI series. *: Significantly different from the 4T1 cells treated with NP (−). #: Significantly different from the 4T1 cells treated with thiol-OS/Au/PEI. †: Significantly different from the 4T1 cells treated with AC300/thiol-OS/Au/PEI. ‡: Significantly different from the 4T1 cells treated with AC600/thiol-OS/Au/PEI. §: Significantly different from the 4T1 cells treated with AC800/thiol-OS/Au/PEI.

https://doi.org/10.1021/acsomega.3c00096
ACS Omega 2023, 8, 9569−9582

are 9−13% and 0.04−0.16, respectively, in the cells treated with all thiol-OS/Au samples. This suggests that the enzyme-like activity of all thiol-OS/Au samples did not damage the nuclei in the absence of X-ray. In the case of 8 Gy of X-ray irradiation, the percentage of damaged cells in the group treated with all the thiol-OS/Au samples is 90−95% and did not differ considerably for all the samples. However, the F.I. of the cells treated with NP (−), AC (−)/thiol-OS/Au, AC300/thiol-OS/Au, AC600/thiol-OS/Au, and AC800/thiol-OS/Au is 8.65, 11.75, 11.95, 10.43, and 10.29 expression of γ-H2AX, respectively, after 15 min of 8 Gy of X-ray irradiation. These results show that 8 Gy of X-ray irradiation induces DNA damage. The induced DNA damage of 4T1 cells treated with AC (−)/thiol-OS/Au and AC300/thiol-OS/Au substantially increased. From the results of NP uptake presented in Table 1, AC (−)/thiol-OS/Au/PEI and AC300/thiol-OS/Au/PEI show a higher cell uptake than AC600/thiol-OS/Au/PEI and AC800/thiol-OS/Au/PEI for 4T1 cells. Additionally, the ROS generation for thiol-OS/Au upon X-ray irradiation indicates high generation ability, as shown in Figure 4. These results also indicate that the AC (−)/thiol-OS/Au/PEI induces DNA damage in 4T1 cells upon X-ray irradiation.

Deactivated Mitochondrial Activity by the Thiol-OS/Au Series. The enzyme-like activity test for evaluating the POD-like activity demonstrated that AC600/thiol-OS/Au/PEI and AC800/thiol-OS/Au/PEI induce ROS formation (Figure 3). Furthermore, the oxidative stress by inorganic and metallic NP has been discussed as a critical mechanism of cell cytotoxicity.[48] For *in vitro* systems, the elevation of intracellular ROS levels elicits a multitude of biological effects that ultimately lead to cell death. Pan et al. reported that Au NPs of diameter 1.4 nm capped with triphenylphosphine monosulfonate were associated with increased ROS production and the loss of mitochondrial potential, leading to necrotic cell death.[15] The necrotic cell death is primarily due to impaired mitochondrial function, leading to elevated intracellular ROS even though the origin of the ROS generation by Au NPs was not clearly demonstrated. Wahab et al. reported that Au NPs of diameter 10−15 nm capped with citrate showed Au NP dose-dependent activity, resulting in a decreased density of cells. The intracellular ROS levels with Au NPs were associated with an upregulation of caspase 3 and 7, leading to apoptosis via mitochondrial dysfunction.[49] Thus, the oxidative stress for ROS generation by Au NPs is associated with protein and lipid oxidation, which profoundly alters the mitochondrial function thought to constitute the central executioner of cell death.[50] In addition, Taggart et al. reported that 1.9 nm AuNPs (AuroVist) caused mitochondrial dysfunction, resulting in the radiosensitization for mitochondria-mediated enhancement in cell death.[51] The mitochondrial membrane stained with TMRE was used to assess mitochondrial activity. Positively charged TMRE interacts in the active mitochondria owing to their negatively maintained mitochondrial membrane charge. However, inactive mitochondria result in the formation of depolarized mitochondria, have a reduced membrane potential, and are unable to accumulate TMRE.

Figure 6A shows the FM images of the NP (−)- and thiol-OS/Au/PEI series-treated 4T1 cells with 0 and 8 Gy on DAY 1 after X-ray irradiation. The 4T1 cells are stained with TMRE, and the F.I. of TMRE is reflected in the increased mitochondrial activity. After 8 Gy of X-ray irradiation, the F.I. of TMRE decreases under all conditions (NP (−) and thiol-OS/Au series). A strong F.I. of TMRE is observed for AC (−)/thiol-OS/Au/PEI-treated 4T1 cells with or without X-ray irradiation.

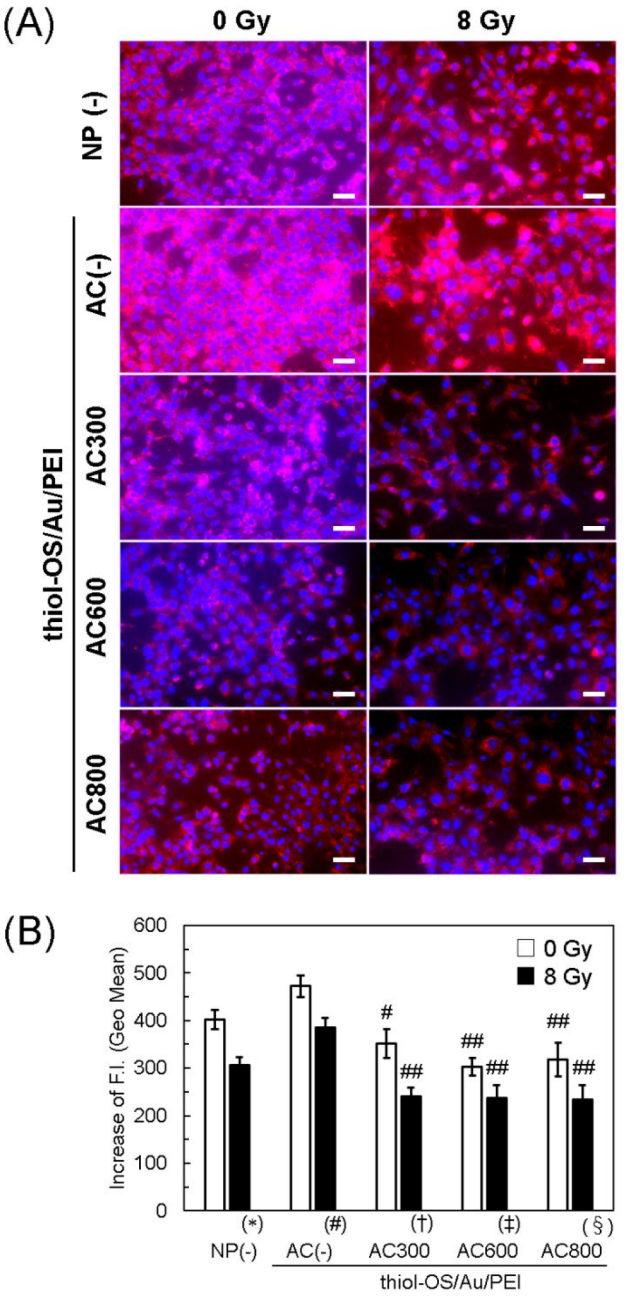

Figure 6. (A) FM images of 4T1 cells at DAY 1 after X-ray irradiation. 4T1 cells were treated with the thiol-OS/Au/PEI series and 0 and 8 Gy X-ray irradiation. Scale bar = 50 μm. (B) Intensity of TMRE stain via the flow cytometric analysis of 4T1 cells treated with the thiol-OS/Au/PEI series upon 0 and 8 Gy X-ray irradiation. Increases in the FL2 channel stained by TMRE were calculated by subtracting the F.I. (geo mean) of the cells treated with NPs and stained with TMRE from the control cells treated with NPs but not stained with TMRE. Each value represents mean ± SD, where n = 3. Concentration of NPs represents AC (−)/thiol-OS/Au, indicating that the concentration of Au is fixed in the thiol-OS/Au/PEI series. *: Significantly different from the 4T1 cells treated with NP (−). #: Significantly different from the 4T1 cells treated with AC (−)/thiol-OS/Au/PEI. †: Significantly different from the 4T1 cells treated with AC300/thiol-OS/Au/PEI. ‡: Significantly different from the 4T1 cells treated with AC600/thiol-OS/Au/PEI. §: Significantly different from the 4T1 cells treated with AC800/thiol-OS/Au/PEI.

https://doi.org/10.1021/acsomega.3c00096
ACS Omega 2023, 8, 9569−9582

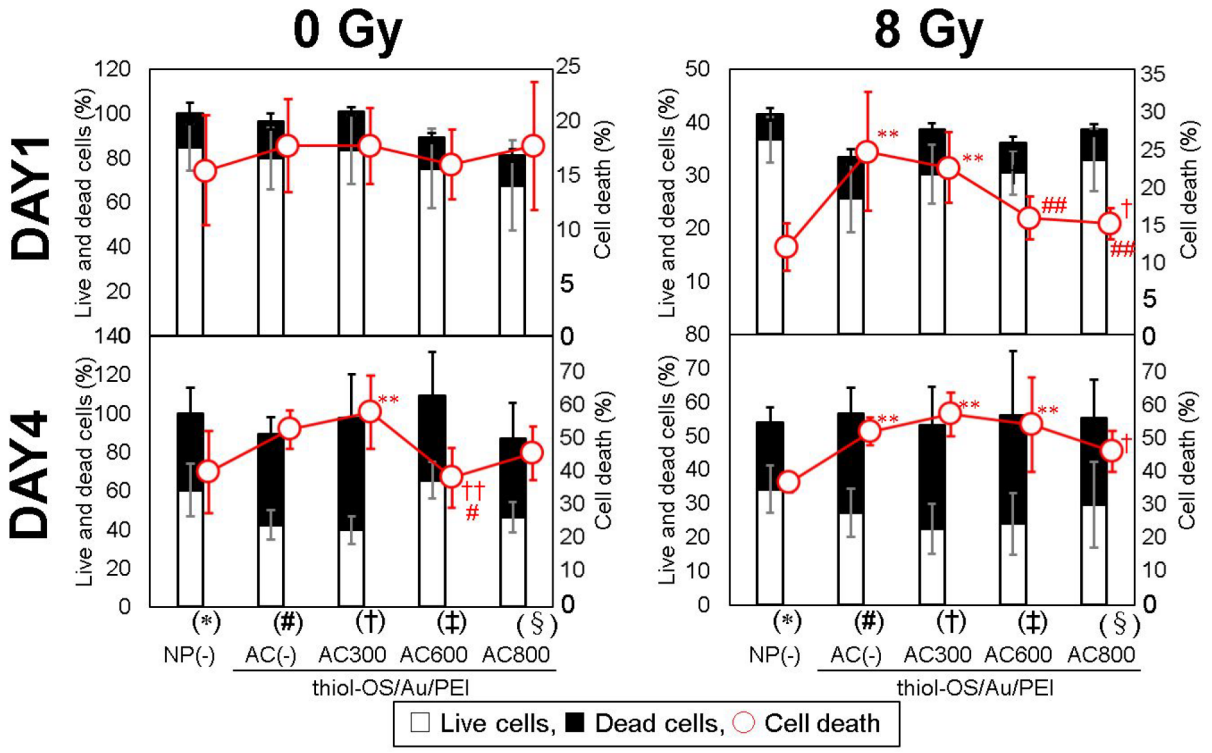

Figure 7. Cell counts and cell viability of the 4T1 cells treated with the thiol-OS/Au/PEI series on DAY 1 and DAY 4 after 0 and 8 Gy X-ray irradiation. Each value represents mean ± SD, where $n = 9$ (three replicates for three independent experiments). Concentration of NPs represent AC (−)/thiol-OS/Au; the concentration of Au is fixed in the thiol-OS/Au/PEI series. #: Significantly different from the 4T1 cells treated with AC (−)/thiol-OS/Au/PEI. †: Significantly different from the 4T1 cells treated with AC300/thiol-OS/Au/PEI. ‡: Significantly different from the 4T1 cells treated with AC600/thiol-OS/Au/PEI. §: Significantly different from the 4T1 cells treated with AC800/thiol-OS/Au/PEI.

Furthermore, we quantified F.I. to evaluate mitochondrial activity in Figure 6B via FCM analyses. On DAY 1, after 8 Gy of X-ray irradiation, we evaluated the mitochondrial activity after treatment at 0 and 8 Gy under all conditions (NP (−) and thiol-OS/Au/PEI series). The data correcting time point was determined on DAY 1 after X-ray irradiation because our previous study showed that the mitochondrial activity for 4T1 cells on DAY 1 after X-ray irradiation changed significantly under several conditions.[11] Figure 6B shows that the mitochondrial activity of the cells treated with thiol-OS/Au/PEI series at 0 and 8 Gy has the same tendency. AC (−)/thiol-OS/Au/PEI treated cells have stronger mitochondrial activity than NP (−)-treated cells. Furthermore, the mitochondrial activity of the cells treated with AC300/thiol-OS/Au/PEI, AC600/thiol-OS/Au/PEI, and AC800/thiol-OS/Au/PEI is significantly weaker than that of the cells with AC (−)/thiol-OS/Au/PEI; the mitochondrial activity of the cells treated with AC (−)/thiol-OS/Au may be higher than that of the others.

Significantly, the weak mitochondrial activity of the cells treated with AC600/thiol-OS/Au/PEI and AC800/thiol-OS/Au/PEI showed good agreement with the POD-like activity of the NPs. However, AC300/thiol-OS/Au did not show POD-like activity, and the mitochondrial activity of these treated cells also decreased, suggesting that not only POD-like activity but also other effects contribute toward the deactivation of the mitochondrial activity. In addition, the thiol-OS/Au/PEI series-treated 4T1 cells are not sensitized by X-rays for mitochondrial damage because the order of damage levels of mitochondria determined via TMRE staining for the thiol-OS/Au/PEI series does not relate to the ROS generation of NPs at 8 Gy X-ray irradiation (Figure 4).

Cell Proliferation and Cell Death Due to the Thiol-OS/Au Series with X-ray Irradiation. Cell counts (live and dead cells) and cell viability counts measured using the trypan blue staining show the effects of X-rays during the very early stages (DAY 1) in Figure 7. Our previous study showed that the cytotoxicity at an early stage could be evaluated via the cell count method.[11] The cell viability of the 4T1 cells treated with the thiol-OS/Au/PEI series does not indicate cytotoxicity in the absence of X-ray irradiation. The active mitochondria evaluated via TMRE staining show that the POD-like activity of NPs (AC600/thiol-OS/Au and AC800/thiol-OS/Au) slightly deactivated the mitochondrial activity without X-ray irradiation. Additionally, these levels of mitochondrial damage by thiol-OS/Au/PEI series do not induce cell death without X-ray irradiation because the cell viability via the cell counting method does not relate to the decreased cell viability. The evaluation results were obtained via cell counting on DAY 1 after 8 Gy of X-ray irradiation, and approximately 40% of the cells (live and dead cells) was observed after X-ray irradiation with or without the NP treatment. The percentages of cell death for the cells treated with AC (−)/thiol-OS/Au/PEI and AC300/thiol-OS/Au/PEI were 24% and 22%, respectively, which were higher than the values for those treated with NP (−) at 8 Gy irradiation (12%). These results show good agreement with the results of DNA damage analysis of the 4T1 cells treated with the thiol-OS/Au/PEI series. The 4T1 cells treated with AC (−)/thiol-OS/Au/PEI and AC300/thiol-OS/Au/PEI showed high DNA damage and induced cell death in the early stage (DAY 1 after X-ray irradiation), indicating that DNA damage could relate to early stage cell death. The rate of early stage cell death determined by

https://doi.org/10.1021/acsomega.3c00096
ACS Omega 2023, 8, 9569−9582

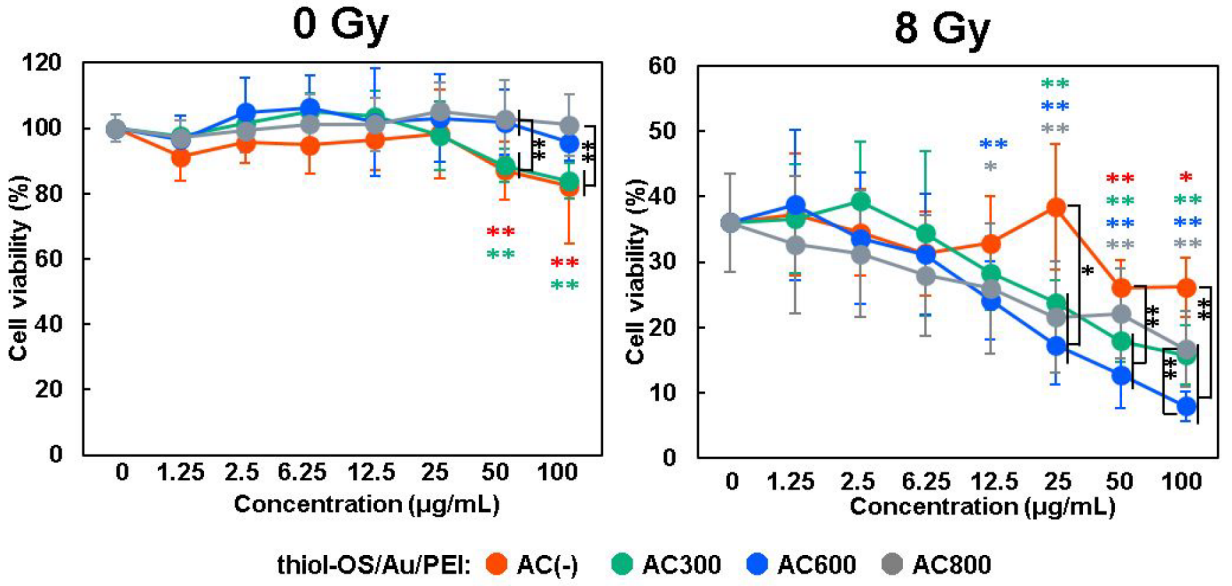

Figure 8. Cell viabilities for the 4T1 cells treated with various concentrations of the thiol-OS/Au series determined by WST-1 assays. Concentration of NPs represents AC (−)/thiol-OS/Au, indicating that the concentration of Au is fixed in AC (−)/thiol-OS/Au/PEI series. Each value represents mean ± SD, where $n = 9$ (three replicates for three independent experiments). *: Significantly different from the 4T1 cells treated with 0 μg/mL of NPs.

cell counting reflected the results of the DNA damage analysis, owing to the irradiation of X-rays and treatment with NPs.

On DAY 4, after 8 Gy of X-ray irradiation, we initially focused on the case without X-ray irradiation. Herein, the cell death percentage of the 4T1 cells treated with NP (−) was less than 40% because the nutrients could not be supplied for survival to the cell under long-term incubation conditions. The 4T1 cells treated with AC (−)/thiol-OS/Au/PEI and AC300/thiol-OS/Au/PEI showed an increase in the cell death ratio. The ratio of cell death for the cells treated with AC600/thiol-OS/Au was 37% and substantially lower than the value for those treated with NP (−) without X-ray irradiation. Next, with 8 Gy of X-ray irradiation, the cell death ratio for the cells treated with AC (−)/thiol-OS/Au, AC300/thiol-OS/Au, and AC600/thiol-OS/Au were 52%, 57%, and 53%, respectively, and considerably higher than those treated with NP (−) at 8 Gy irradiation (36%). In addition, the number of live cells treated with AC300/thiol-OS/Au and AC600/thiol-OS/Au was the lowest, accounting for approximately 20% of the cells, indicating the application potential in radiotherapy. The result of WST-1 showed the highest decrease of cell viability for AC600/thiol-OS/Au/PEI-treated 4T1 cells, showing the same tendency as that for the cell counting method, which will be described in the part of cell viability by the WST-1 assay for thiol-OS/Au series with X-ray irradiation.

Notably, under the long-term cell culture condition (DAY 4), the cytotoxicity of AC (−)/thiol-OS/Au/PEI decreased with 8 Gy X-ray irradiation. Contrarily, the cytotoxicity of AC600/thiol-OS/Au/PEI increased with 8 Gy X-ray irradiation. In addition, the comparison of the effects of 0 and 8 Gy irradiation for the 4T1 cells treated with AC600/thiol-OS/Au on DAY 4 showed an opposite tendency (decrease and increase in cell death for 0 and 8 Gy, respectively), suggesting that AC600/thiol-OS/Au/PEI exhibits a different behavior in 4T1 cells with 0 and 8 Gy X-ray irradiation.

Cell Viability by WST-1 Assay for Thiol-OS/Au Series with X-ray Irradiation. Figure 8 shows the results of the WST-1 assay on DAY 4 after X-ray irradiation. The 4T1 cells for thiol-OS/Au/PEI series without X-ray irradiation (0 Gy) did not show cell cytotoxicity up to 25 μg/mL. Even at concentrations up to 100 μg/mL, no cytotoxicity is observed, except for AC (−)/thiol-OS/Au/PEI and AC300/thiol-OS/Au/PEI. For AC (−)/thiol-OS/Au/PEI and AC300/thiol-OS/Au/PEI, the high concentrations of 50 and 100 μg/mL result in a slight decrease in cell viability under long-term cell culture conditions. This result, in which AC (−)/thiol-OS/Au/PEI and AC300/thiol-OS/Au/PEI show an increase in the cell death ratio on DAY 4 without X-ray irradiation by cell counts and cell viability counts, also shows the same tendency as the results of cell counts. The slight decrease in cell viability for the 4T1 cells treated with AC (−)/thiol-OS/Au/PEI and AC300/thiol-OS/Au/PEI implies the cytotoxicity of the modified-PEI on NPs[52] because AC (−)/thiol-OS/Au/PEI and AC300/thiol-OS/Au/PEI are absorbed more than AC600/thiol-OS/Au/PEI and AC800/thiol-OS/Au/PEI (Table 1), indicating that the cytotoxicity of PEI[52,53] accelerated the PEI-modified NP uptake.

For the 8 Gy X-ray irradiation of the 4T1 cells treated with thiol-OS/Au series, the cell viability decreased noticeably to 36% even without NP treatment (NP(−)). In addition, AC (−)/thiol-OS/Au series caused dose-dependent cell deaths at NP concentrations. For AC (−)/thiol-OS/Au/PEI and AC300/thiol-OS/Au/PEI, cytotoxicity was gradually shown at a concentration of 50 and 25 μg/mL of NPs, respectively. AC600/thiol-OS/Au/PEI and AC800/thiol-OS/Au/PEI exhibited cytotoxicity more significantly (24% and 26% cell viability, respectively) for a low concentration of 12.5 μg/mL of the NPs. The order of cell viability of 4T1 cells for thiol-OS/Au/PEI series at the concentration of 12.5 μg/mL of the NPs was AC (−)/thiol-OS/Au/PEI > AC300/thiol-OS/Au/PEI > AC800/thiol-OS/Au/PEI > AC600/thiol-OS/Au/PEI. In addition, 25 μg/mL of AC600/thiol-OS/Au/PEI showed higher cytotoxicity than AC (−)/thiol-OS/Au/PEI, and 100 μg/mL of AC600/thiol-OS/Au/PEI showed higher cytotoxicity than other NPs, significantly. Notably, the viability of cells treated with AC (−)/thiol-OS/Au/PEI determined by the WST-1 assay showed high cell viability even though AC (−)/thiol-OS/Au/

https://doi.org/10.1021/acsomega.3c00096
ACS Omega 2023, 8, 9569−9582

PEI possessed ROS generation properties, particularly for ·OH and $O_2{\cdot}^-$ via X-ray irradiation (Figure 4A). However, the cells treated with AC600/thiol-OS/Au/PEI showed low cell viability.

From the perspective of enzyme-like activity, AC600/thiol-OS/Au/PEI possesses POD-like activity, indicating the generation of ·OH under acidic conditions (Figure 3). These results suggested that the cytotoxicity with X-ray irradiation was affected more effectively by the enzyme-like ·OH generation than by X-ray irradiation. The enzyme-like ·OH generation suggested a synergistic sensitizing effect of X-ray irradiation for 4T1 cells. The enzyme-like activity of AC600/thiol-OS/Au shows different POD- and CAT-like activities depending on acidic and basic pH, respectively, in Figure 3. We hypothesized that, by 8 Gy irradiation, the 4T1 cells transform into senescent cells,[11] exhibiting the possibility for the intracellular pH being lowered by lysosomal membrane damage.[54] The condition of the senescent cells caused by X-ray irradiation results in POD-like activity, suggesting the gradually induced oxidative damage to 4T1 cells.

CONCLUSIONS

Herein, we evaluated the radiosensitizing effects of different Au states in a thiol-OS/Au series, focusing on the enzyme-like activity and ROS generation under X-ray irradiation for 4T1 cells *in vitro*. Considering the enzyme-like activity of the thiol-OS/Au series, AC (−)/thiol-OS/Au showed SOD-like activity under neutral and basic pH conditions. AC600/thiol-OS/Au showed the highest POD activity among the analyzed thiol-OS/Au samples, suggesting that Au NPs with smaller sizes ($0.8 \pm 0.3/3.3 \pm 1.2$ nm) and Au(0) state were favorable for POD-like activity. Additionally, AC600/thiol-OS/Au exhibited POD- and CAT-like activities under acidic and basic conditions, respectively. In the thiol-OS/Au series, AC (−)/thiol-OS/Au showed higher ROS-sensitizing ability compared to other thiol-OS/Au samples and caused a high DNA damage. The cytotoxicity on DAY 4 after the X-ray irradiation (8 Gy) of cells treated with thiol-OS/Au series was in the order of AC600/thiol-OS/Au/PEI > AC800/thiol-OS/Au/PEI > AC300/thiol-OS/Au/PEI > AC (−)/thiol-OS/Au/PEI, even when the efficiency of cellar uptake of Au was considered. The results indicate that the X-ray-sensitizing ability of samples to impart cytotoxicity for 4T1 cells had a higher correlation with POD-like activity than with ROS generation by X-ray irradiation. Furthermore, the increase in the POD-like activity of the thiol-OS/Au series indicated the loss of mitochondrial membrane potential; however, mitochondrial damage did not directly affect cell death. These results proved that the POD-like activity of the Au state (Au NP) is beneficial for applying Au nanomaterials as radiosensitizers in X-ray radiotherapy. In the future, we will expand the evaluation of thiol-OS/Au series behavior an *in vivo* study. This perspective could be applied to other metal-based NPs with potential radiosensitizing effects. Therefore, this study provides an effective design strategy for efficient radiosensitizing nanomaterials.

ASSOCIATED CONTENT

Supporting Information

The Supporting Information is available free of charge at https://pubs.acs.org/doi/10.1021/acsomega.3c00096.

Superoxide dismutase (SOD)-like activity of thiol-OS without Au at pH 7.4, SOD-like activity of thiol-OS/Au series at pH 7.4 in the absence of NADH and PMS, hydrodynamic diameters and zeta potentials of thiol-OS/Au series using dynamic light scattering (DLS) measurement (PDF)

AUTHOR INFORMATION

Corresponding Author

Michihiro Nakamura − *Department of Organ Anatomy & Nanomedicine, Graduate School of Medicine, Yamaguchi University, Ube, Yamaguchi 755-8505, Japan; Core Clusters for Research Initiatives of Yamaguchi University, Ube, Yamaguchi 755-8505, Japan;* orcid.org/0000-0002-9216-3215; Phone: +81-836-22-2202; Email: nakam@yamaguchi-u.ac.jp

Authors

Chihiro Mochizuki − *Department of Organ Anatomy & Nanomedicine, Graduate School of Medicine, Yamaguchi University, Ube, Yamaguchi 755-8505, Japan; Core Clusters for Research Initiatives of Yamaguchi University, Ube, Yamaguchi 755-8505, Japan;* orcid.org/0000-0002-7699-0157

Junna Nakamura − *Department of Organ Anatomy & Nanomedicine, Graduate School of Medicine, Yamaguchi University, Ube, Yamaguchi 755-8505, Japan; Core Clusters for Research Initiatives of Yamaguchi University, Ube, Yamaguchi 755-8505, Japan;* orcid.org/0000-0003-1547-7357

Complete contact information is available at: https://pubs.acs.org/10.1021/acsomega.3c00096

Author Contributions

C.M. performed the synthesis and characterization of thiol-OS/Au, conducted the cell experiments, and drafted the manuscript. J.N. performed the cell experiments. M.N. supervised this work.

Funding

This study was supported in part by JSPS KAKENHI (Grant-in-Aid for Early-Career Scientists (No. 20 K15322) and Grant-in-Aid for Scientific Research (B) (No. 20H03625)).

Notes

The authors declare no competing financial interest.

ACKNOWLEDGMENTS

We appreciate the assistance with electron microscopic observations by Dr. Azumi Yoshimura.

ABBREVIATIONS

AC, air calcination; APF, aminophenyl fluorescein; CAT, catalase; DAPI, 4′,6-diamidino-2-phenylindole; DHE, dihydroethidium; DLS, dynamic light scattering; DNA, deoxyribonucleic acid; DSB, double-strand break; DW, distilled water; FCM, flow cyclometry; F.I., fluorescence intensity; FM, fluorescence microscopy; ICP-OES, inductively coupled plasma optical emission spectroscopy; IR, ionizing radiation; NADH, nicotinamide adenine dinucleotide; NBT, nitro blue tetrazolium; NP, nanoparticle; OS, organosilica; PEI, polyethylenimine; PMS, phenazine methosulfate; POD, peroxidase; ROS, reactive oxygen species; SOD, superoxide dismutase; TEM, transmission electron microscopy; TMB, 3,3,5,5-tetramethylbenzidine; TMRE, tetramethylrhodamine methyl ester; XPS, X-ray photoelectron spectroscopy

https://doi.org/10.1021/acsomega.3c00096
ACS Omega 2023, 8, 9569−9582

REFERENCES

(1) Delaney, G.; Jacob, S.; Featherstone, C.; Barton, M. The Role of Radiotherapy in Cancer Treatment: Estimating Optimal Utilization from a Review of Evidence-Based Clinical Guidelines. *Cancer* **2005**, *104*, 1129−1137.

(2) Wang, H.; Mu, X.; He, H.; Zhang, X.-D. Cancer Radiosensitizers. *Trends Pharmacol. Sci.* **2018**, *39*, 24−48.

(3) Cross, C. E.; Halliwell, B.; Borish, E. T.; Pryor, W. A.; Ames, B. N.; Saul, R. L.; McCord, J. M.; Harman, D. Oxygen Radicals and Human Disease. Davis Conference. *Ann. Int. Med. Davis Conf.* **1987**, *107*, 526−545.

(4) Schieber, M.; Chandel, N. S. ROS Function in Redox Signaling and Oxidative Stress. *Curr. Biol.* **2014**, *24*, R453−R462.

(5) Mah, L. J.; El-Osta, A.; Karagiannis, T. C. Γh2AX: A Sensitive Molecular Marker of DNA Damage and Repair. *Leukemia* **2010**, *24*, 679−686.

(6) Mochizuki, C.; Nakamura, J.; Nakamura, M. Development of Non-Porous Silica Nanoparticles towards Cancer Photo-Theranostics. *Biomedicines* **2021**, *9*, 73.

(7) Nakamura, M.; Ishimura, K. One-Pot Synthesis and Characterization of Three Kinds of Thiol - Organosilica Nanoparticles. *Langmuir* **2008**, *24*, 5099−5108.

(8) Nakamura, M. Organosilica Nanoparticles and Medical Imaging. *Enzymes* **2018**, *44*, 137−173.

(9) Nakamura, M.; Hayashi, K.; Nakamura, J.; Mochizuki, C.; Murakami, T.; Miki, H.; Ozaki, S.; Abe, M. Near-Infrared Fluorescent Thiol-Organosilica Nanoparticles That Are Functionalized with IR-820 and Their Applications for Long-Term Imaging of in Situ Labeled Cells and Depth-Dependent Tumor in Vivo Imaging. *Chem. Mater.* **2020**, *32*, 7201−7214.

(10) Nakamura, M.; Hayashi, K.; Nakano, M.; Kanadani, T.; Miyamoto, K.; Kori, T.; Horikawa, K. Identification of Polyethylene Glycol-Resistant Macrophages on Stealth Imaging in Vitro Using Fluorescent Organosilica Nanoparticles. *ACS Nano* **2015**, *9*, 1058−1071.

(11) Mochizuki, C.; Kayabe, Y.; Nakamura, J.; Igase, M.; Mizuno, T.; Nakamura, M. Surface Functionalization of Organosilica Nanoparticles With Au Nanoparticles Inhibits Cell Proliferation and Induces Cell Death in 4T1Mouse Mammary Tumor Cells for DNA and Mitochondrial-Synergized Damage in Radiotherapy. *Front. Chem.* **2022**, *10*, 1.

(12) Regulla, D. F.; Hieber, L. B.; Seidenbusch, M. Physical and Biological Interface Dose Effects in Tissue Due to X-Ray- Induced Release of Secondary Radiation from Metallic Gold Surfaces. *Radiat. Res.* **1998**, *150*, 92−100.

(13) Cheng, N. N.; Starkewolf, Z.; Davidson, R. A.; Sharmah, A.; Lee, C.; Lien, J.; Guo, T. Chemical Enhancement by Nanomaterials under X-Ray Irradiation. *J. Am. Chem. Soc.* **2012**, *134*, 1950−1953.

(14) Her, S.; Jaffray, D. A.; Allen, C. Gold Nanoparticles for Applications in Cancer Radiotherapy: Mechanisms and Recent Advancements. *Adv. Drug Delivery Rev.* **2017**, *109*, 84−101.

(15) Pan, Y.; Leifert, A.; Ruau, D.; Neuss, S.; Bornemann, J.; Schmid, G.; Brandau, W.; Simon, U.; Jahnen-Dechent, W. Gold Nanoparticles of Diameter 1.4 Nm Trigger Necrosis by Oxidative Stress and Mitochondrial Damage. *Small* **2009**, *5*, 2067−2076.

(16) Carlson, C.; Hussain, S. M.; Schrand, A. M.; Braydich-Stolle, L. K.; Hess, K. L.; Jones, R. L.; Schlager, J. J. Unique Cellular Interaction of Silver Nanoparticles: Size-Dependent Generation of Reactive Oxygen Species. *J. Phys. Chem. B* **2008**, *112*, 13608−13619.

(17) Xia, T.; Kovochich, M.; Brant, J.; Hotze, M.; Sempf, J.; Oberley, T.; Sioutas, C.; Yeh, J. I.; Wiesner, M. R.; Nel, A. E. Comparison of the Abilities of Ambient and Manufactured Nanoparticles to Induce Cellular Toxicity According to an Oxidative Stress Paradigm. *Nano Lett.* **2006**, *6*, 1794−1807.

(18) Haruta, M.; Kobayashi, T.; Sano, H.; Yamada, N. Novel Gold Catalysts for the Oxidation of Carbon Monoxide at a Temperature Far Below 0 °C. *Chem. Lett.* **1987**, *16*, 405−408.

(19) Hutchings, G. J. Vapor Phase Hydrochlorination of Acetylene: Correlation of Catalytic Activity of Supported Metal Chloride Catalysts. *J. Catal.* **1985**, *96*, 292−295.

(20) Ishida, T.; Murayama, T.; Taketoshi, A.; Haruta, M. Importance of Size and Contact Structure of Gold Nanoparticles for the Genesis of Unique Catalytic Processes. *Chem. Rev.* **2020**, *120*, 464−525.

(21) Taketoshi, A.; Haruta, M. Size- and Structure-Specificity in Catalysis by Gold Clusters. *Chem. Lett.* **2014**, *43*, 380−387.

(22) Wang, H.; Wan, K.; Shi, X. Recent Advances in Nanozyme Research. *Adv. Mater.* **2019**, *31*, 1805368.

(23) Chen, Z.; Yin, J. J.; Zhou, Y. T.; Zhang, Y.; Song, L.; Song, M.; Hu, S.; Gu, N. Dual Enzyme-like Activities of Iron Oxide Nanoparticles and Their Implication for Diminishing Cytotoxicity. *ACS Nano* **2012**, *6*, 4001−4012.

(24) Lou-Franco, J.; Das, B.; Elliott, C.; Cao, C. Gold Nanozymes: From Concept to Biomedical Applications. *Nano-Micro Lett.* **2021**, *13*, 10.

(25) Lin, Y.; Ren, J.; Qu, X. Nano-Gold as Artificial Enzymes: Hidden Talents. *Adv. Mater.* **2014**, *26*, 4200−4217.

(26) Zhang, X.; Zhang, C.; Cheng, M.; Zhang, Y.; Wang, W.; Yuan, Z. Dual PH-Responsive "Charge-Reversal like" Gold Nanoparticles to Enhance Tumor Retention for Chemo-Radiotherapy. *Nano Res.* **2019**, *12*, 2815−2826.

(27) Li, J.; Liu, W.; Wu, X.; Gao, X. Mechanism of PH-Switchable Peroxidase and Catalase-like Activities of Gold, Silver, Platinum and Palladium. *Biomaterials.* **2015**, *48*, 37−44.

(28) He, W.; Zhou, Y. T.; Wamer, W. G.; Hu, X.; Wu, X.; Zheng, Z.; Boudreau, M. D.; Yin, J. J. Intrinsic Catalytic Activity of Au Nanoparticles with Respect to Hydrogen Peroxide Decomposition and Superoxide Scavenging. *Biomaterials* **2013**, *34*, 765−773.

(29) Gao, L.; Zhuang, J.; Nie, L.; Zhang, J.; Zhang, Y.; Gu, N.; Wang, T.; Feng, J.; Yang, D.; Perrett, S.; Yan, X. Intrinsic Peroxidase-like Activity of Ferromagnetic Nanoparticles. *Nat. Nanotechnol.* **2007**, *2*, 577−583.

(30) Tao, Y.; Lin, Y.; Huang, Z.; Ren, J.; Qu, X. Incorporating Graphene Oxide and Gold Nanoclusters: A Synergistic Catalyst with Surprisingly High Peroxidase-like Activity over a Broad PH Range and Its Application for Cancer Cell Detection. *Adv. Mater.* **2013**, *25*, 2594−2599.

(31) Wang, Z.; Dong, K.; Liu, Z.; Zhang, Y.; Chen, Z.; Sun, H.; Ren, J.; Qu, X. Activation of Biologically Relevant Levels of Reactive Oxygen Species by Au/g-C3N4 Hybrid Nanozyme for Bacteria Killing and Wound Disinfection. *Biomaterials* **2017**, *113*, 145−157.

(32) Biswas, S.; Tripathi, P.; Kumar, N.; Nara, S. Gold Nanorods as Peroxidase Mimetics and Its Application for Colorimetric Biosensing of Malathion. *Sensors Actuators, B Chem.* **2016**, *231*, 584−592.

(33) McVey, C.; Logan, N.; Thanh, N. T. K.; Elliott, C.; Cao, C. Unusual Switchable Peroxidase-Mimicking Nanozyme for the Determination of Proteolytic Biomarker. *Nano Res.* **2019**, *12*, 509−516.

(34) Bhagat, S.; Srikanth Vallabani, N. V.; Shutthanandan, V.; Bowden, M.; Karakoti, A. S.; Singh, S. Gold Core/Ceria Shell-Based Redox Active Nanozyme Mimicking the Biological Multienzyme Complex Phenomenon. *J. Colloid Interface Sci.* **2018**, *513*, 831−842.

(35) Mochizuki, C.; Nakamura, J.; Nakamura, M. Photostable and Biocompatible Luminescent Thiol-Terminated Organosilica Nanoparticles with Embedded Au(I)-Thiolate Complexes for Fluorescent Microscopic Imaging. *ACS Appl. Nano Mater.* **2021**, *4*, 13305−13318.

(36) Ponti, V.; Dianzani, M. U.; Cheeseman, K.; Slater, T. F. Studies on the Reduction of Nitroblue Tetrazolium Chloride Mediated through the Action of NADH and Phenazine Methosulphate. *Chem. Biol. Interact.* **1978**, *23*, 281−291.

(37) Mochizuki, C.; Nakamura, J.; Nakamura, M. Preparation of Fetal Bovine Serum-Copper Phosphate Hybrid Particles under Cell Culture Conditions for Cancer Cell Treatment. *ACS Omega* **2022**, *7*, 29495−29501.

(38) Wang, C.; Li, Y.; Yang, W.; Zhou, L.; Wei, S. Nanozyme with Robust Catalase Activity by Multiple Mechanisms and Its Application for Hypoxic Tumor Treatment. *Adv. Healthc. Mater.* **2021**, *10*, 2100601.

https://doi.org/10.1021/acsomega.3c00096
ACS Omega 2023, 8, 9569−9582

(39) Nakamura, M. Biomedical Applications of Organosilica Nanoparticles toward Theranostics. *Nanotechnol. Rev.* **2012**, *1*, 469−491.
(40) Luo, Z.; Yuan, X.; Yu, Y.; Zhang, Q.; Leong, D. T.; Lee, J. Y.; Xie, J. From Aggregation-Induced Emission of Au(I)-Thiolate Complexes to Ultrabright Au(0)@Au(I)-Thiolate Core-Shell Nanoclusters. *J. Am. Chem. Soc.* **2012**, *134*, 16662−16670.
(41) Senkevich, J. J.; Mitchell, C. J.; Yang, G. R.; Lu, T. M. Surface Chemistry of Mercaptan and Growth of Pyridine Short-Chain Alkoxy Silane Molecular Layers. *Langmuir* **2002**, *18*, 1587−1594.
(42) Li, J.; Liu, W.; Wu, X.; Gao, X. Mechanism of PH-Switchable Peroxidase and Catalase-like Activities of Gold, Silver, Platinum and Palladium. *Biomaterials* **2015**, *48*, 37−44.
(43) Sun, Y.; Liu, X.; Wang, L.; Xu, L.; Liu, K.; Xu, L.; Shi, F.; Zhang, Y.; Gu, N.; Xiong, F. High-Performance SOD Mimetic Enzyme Au@Ce for Arresting Cell Cycle and Proliferation of Acute Myeloid Leukemia. *Bioact. Mater.* **2022**, *10*, 117−130.
(44) Warburg, O. On the Origin of Cancer Cells. *Science* **1956**, *123*, 309−314.
(45) Misawa, M.; Takahashi, J. Generation of Reactive Oxygen Species Induced by Gold Nanoparticles under X-Ray and UV Irradiations. *Nanomed. Nanotechnol., Biol. Med.* **2011**, *7*, 604−614.
(46) Wang, L.; Zhang, T.; Huo, M.; Guo, J.; Chen, Y.; Xu, H. Construction of Nucleus-Targeting Iridium Nanocrystals for Photonic Hyperthermia-Synergized Cancer Radiotherapy. *Small* **2019**, *15*, 1903254.
(47) Goudarzi, M.; Salavati-Niasari, M.; Amiri, M. Effective Induction of Death in Breast Cancer Cells with Magnetite NiCo 2 O 4 /NiO Nanocomposite. *Compos. Part B Eng.* **2019**, *166*, 457−463.
(48) Nel, A.; Xia, T.; Mädler, L.; Li, N. Toxic Potential of Materials at the Nanolevel. *Science* **2006**, *311*, 622−627.
(49) Wahab, R.; Dwivedi, S.; Khan, F.; Mishra, Y. K.; Hwang, I. H.; Shin, H. S.; Musarrat, J.; Al-Khedhairy, A. A. Statistical Analysis of Gold Nanoparticle-Induced Oxidative Stress and Apoptosis in Myoblast (C2C12) Cells. *Colloids Surf., B* **2014**, *123*, 664−672.
(50) Kroemer, G. Mitochondrial Implication in Apoptosis. Towards an Endosymbiont Hypothesis of Apoptosis Evolution. *Cell Death Differ.* **1997**, *4*, 443−456.
(51) Taggart, L. E.; McMahon, S. J.; Currell, F. J.; Prise, K. M.; Butterworth, K. T. The Role of Mitochondrial Function in Gold Nanoparticle Mediated Radiosensitisation. *Cancer Nanotechnol.* **2014**, *5*, 5.
(52) Nakamura, M.; Nakamura, J.; Mochizuki, C.; Kuroda, C.; Kato, S.; Haruta, T.; Kakefuda, M.; Sato, S.; Tamanoi, F.; Sugino, N. Analysis of Cell-Nanoparticle Interactions and Imaging of in Vitro Labeled Cells Showing Barcorded Endosomes Using Fluorescent Thiol-Organosilica Nanoparticles Surface-Functionalized with Polyethyleneimine. *Nanoscale Adv.* **2022**, *4*, 2682−2703.
(53) Fischer, D.; Bieber, T.; Li, Y.; Elsässer, H. P.; Kissel, T. A Novel Non-Viral Vector for DNA Delivery Based on Low Molecular Weight, Branched Polyethylenimine: Effect of Molecular Weight on Transfection Efficiency and Cytotoxicity. *Pharm. Res.* **1999**, *16*, 1273−1279.
(54) Johmura, Y.; Yamanaka, T.; Omori, S.; Wang, T. W.; Sugiura, Y.; Matsumoto, M.; Suzuki, N.; Kumamoto, S.; Yamaguchi, K.; Hatakeyama, S.; Takami, T.; Yamaguchi, R.; Shimizu, E.; Ikeda, K.; Okahashi, N.; Mikawa, R.; Suematsu, M.; Arita, M.; Sugimoto, M.; Nakayama, K. I.; Furukawa, Y.; Imoto, S.; Nakanishi, M. Senolysis by Glutaminolysis Inhibition Ameliorates Various Age-Associated Disorders. *Science* **2021**, *371*, 265−270.

https://doi.org/10.1021/acsomega.3c00096
ACS Omega 2023, 8, 9569−9582